Thickness and Air Gap Dependence of Macrovoid Evolution in Phase-Inversion Asymmetric Hollow Fiber Membranes

ARTICLE *in* INDUSTRIAL & ENGINEERING CHEMISTRY RESEARCH · SEPTEMBER 2006

Impact Factor: 2.59 · DOI: 10.1021/ie0606587

2 AUTHORS:

Natalia Widjojo
BASF South East Asia, Singapore
24 PUBLICATIONS **580** CITATIONS
SEE PROFILE

Tai-Shung Chung
National University of Singapore
727 PUBLICATIONS **19,578** CITATIONS
SEE PROFILE

SEPARATIONS

Thickness and Air Gap Dependence of Macrovoid Evolution in Phase-Inversion Asymmetric Hollow Fiber Membranes

Natalia Widjojo and Tai-Shung Chung*

Department of Chemical and Biomolecular Engineering, National University of Singapore, 10 Kent Ridge Crescent, Singapore 117602

We have studied, for the first time, the effects of spinneret dimension and its coupling effect with air gap distance on macrovoid evolution. Spinnerets with different annulus gaps, i.e., from 0.05 to 0.50 mm, were fabricated. Hollow fiber membranes spun from thinner spinneret annulus gaps show only inward-pointed long, teardrop, and elliptical shape macrovoids, while those spun from thicker annulus gaps have both inward- and outward-pointed macrovoids. On the basis of SEM examination, it is concluded that nonsolvent intrusion due to local surface instability and skin rupture accounts for most inward- and outward-pointed long macrovoid formation, while the diffusion mechanism with the aid of solutocapillary convection possibly accounts for the formation of small teardrop and elliptical shape macrovoids. In addition, the number of inward-pointed macrovoids increases, while the number of outward-pointed macrovoids decreases with an increase in air gap distance. Clearly, many forces affecting macrovoid formation compete with one another starting from within the spinneret through the air gap region. It is found that (1) the shear stresses developed within the thinner spinneret annulus gaps, (2) the gravity-induced elongational drawing, and (3) the moisture-induced partial phase separation in the air gap region all hinder the nonsolvent intrusion and suppress outward-pointed macrovoid formation. The solutocapillary convection may prevail in thicker annulus gaps and longer air gap distances, and most likely accounts for the formation of small inward-pointed teardrop and elliptical shape macrovoids.

1. Introduction

Macrovoid formation in textile fiber and membrane fabrication via phase inversion has been considered an undesirable structural irregularity.[1−3] The presence of macrovoids in the membranes provides weak mechanical points leading to membrane failure when operating at high pressures. The origin of macrovoids is one of the most controversial issues and has been heavily debated in the past four decades among membrane scientists.[4−30] Some early researchers believed it most likely originates from an instantaneous liquid−liquid demixing and the nucleation of droplets in the polymer-lean phase based on the diffusion-driven mechanism,[4−10] while others considered that it more likely starts from a local surface instability, skin rupture and solvent intrusion, followed by the nucleation of droplets in the polymer-lean phase.[1,13−17] References 7, 14, and 16 may be the best representatives of each side. Other mechanisms such as Marangoni effects[18] and osmosis pressure[19] had also been proposed. Krantz and co-workers believe neither diffusion nor Marangoni effects alone can account for the explosive growth of macrovoids;[20,21] they proposed the solutocapillary convection mechanism, which consists of diffusion and Marangoni force generated by surface tension gradients.[22,23] As a result, two main mechanisms are currently favored for macrovoid formation: (1) the diffusion mechanism with the aid of solutocapillary convection and (2) local surface instability, skin rupture, and solvent intrusion. Both hypotheses have significant literature support.[24−30] Clearly, macrovoid formation is complicated because it possibly involves several different mechanisms occurring simultaneously.

Several approaches have been demonstrated to suppress macrovoids, such as (1) the use of high polymer concentration solutions,[3] (2) the addition of high-viscosity components,[31,32] (3) the induction of gelation,[33] (4) the delayed demixing,[34] (5) the choice of nonsolvents with reduced coagulation rate or increased coagulation value,[10,16] (6) the introduction of moisture,[35,36] (7) the addition of surfactants,[37] (8) an increase in the coagulation bath temperature,[38] (9) spinning at high shear rates,[39] and (10) using a high elongational draw ratio.[40]

Recently Vogrin et al.[41] and our research group[42] have discovered the thickness dependence of macrovoid evolution during the phase inversion of asymmetric flat membranes. We observed a critical structure-transition thickness, L_c, which indicates the transition of membrane morphology from a spongelike to a fingerlike structure with an increase in membrane thickness. Below L_c, membranes show a fully spongelike cross section structure, while above L_c membranes exhibit a mainly fingerlike macrovoid structure. Their works inspire us to examine if the same phenomena can be observed in hollow fiber membranes and the fiber spinning process makes macrovoid evolution more complicated. We specifically focus our study on the effects of spinneret dimension and its coupling effect with air gap distance on macrovoid evolution. To our knowledge, no such study has been reported in the literature.

This study is important because, in comparison to flat sheet membranes, the hollow fiber configuration is a favorite choice for membrane separation owing to its large membrane area per

* To whom correspondence should be addressed. Fax: (65)-67791936. E-mail: chencts@nus.edu.sg.

10.1021/ie0606587 CCC: $33.50
Published on Web 09/09/2006

Table 1. Spinneret Identification and Dimensions

dimension	spinneret A	B	C	D	E
outer diameter (o.d., mm)	0.70	0.85	0.81	1.20	1.50
inner diameter (i.d., mm)	0.50	0.50	0.30	0.50	0.50
channel thickness (ΔD, mm)	0.10	0.175	0.25	0.35	0.50

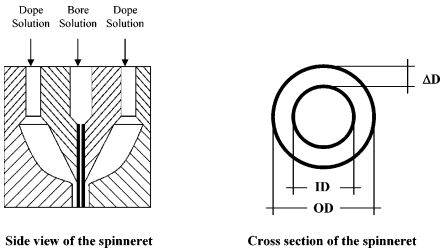

unit volume of membrane material.[43] However, the fabrication of asymmetric hollow fibers is more complicated than that of asymmetric flat membranes. The former has more factors controlling membrane morphology during the phase inversion than the latter. For example, there are two coagulations taking place in the hollow fiber spinning (internal and external surfaces), while there is only one major coagulation surface for an asymmetric flat sheet membrane. In addition, if liquids are used as bore fluids, the internal coagulation process for a hollow fiber may start immediately after exiting from a spinneret and then is followed by the external coagulation process, while there is usually a waiting period for an asymmetric flat sheet membrane before immersion in the coagulant. Furthermore, die swell occurs in the hollow fiber spinning because of fluid relaxation and the existence of a free moving membrane surface in the air gap region. As a result, the macrovoid formation is more complicated in the hollow fiber spinning process than in asymmetric flat membranes. Up to the present, only a small number of researchers have noticed the effects of air gap distance on macrovoids,[35,36] but the effects of fluid behavior within the spinneret on macrovoid formation have been almost entirely ignored. Part of the objective of this paper is to systematically study this issue and reveal its importance in membrane formation.

2. Experimental Section

In this work, P84 (BTDA−TDI/MDI, copolyimide of 3,3′,4,4′-benzophenone tetracarboxylic dianhydride and 80% methylphenylenediamine + 20% methylenediamine), a recently commercially available polyimide, was chosen because it has been used in our previous work for the flat asymmetric membrane study.[42] This material was purchased from HP Polymer Gmbh, Austria.

Spinnerets with different annulus gaps of flow channels were fabricated and are listed in Table 1. For readers' information, a typical spinneret design used in this study is illustrated in Table 1. It has been recognized that, for a flow in the capillary, an L/D (D is the diameter of flow channel and L is the length of flow channel in the spinneret) ratio greater than 10 might be necessary to provide a fully developed flow.[44,45] The $L/\Delta D$ (ΔD = annulus gap) ratios used in our spinnerets are always greater than 20 to ensure a steady shear flow developed in the spinneret before exiting.

The experimental setup and spinning procedure for these fibers have been disclosed elsewhere.[30,32,40] The hollow fiber membranes were prepared using a dope composition of 26/64/10 (wt %) P84/*N*-methylpyrrollidone (NMP)/ethanol based on the phase diagram of this ternary system.[46] An ARES Rheometric Scientific Rheometer was utilized to determine the shear stress of the dope solution as a function of shear rate. The experiment was carried out using a 25 mm cone plate at 25 °C and the steady-state shear was measured in the range of 1−100 s^{-1}. The power-law model[47,48] was applied to fit the rheological data, and a relationship between shear stress τ (N m^{-2}) and shear rate γ (s^{-1}) was obtained as follows:

$$\tau = 13.22|\gamma|^{0.9903} \quad (1)$$

The shear stress and rate at the outer wall of a spinneret can be predicted by the above equation from the velocity profile. Table 2 summarizes the spinning conditions used in this work. The relative humidity during spinning was 65%. Pure water was employed as the external and internal coagulants.

Table 2. Spinning Conditions for P84 Copolyimide Hollow Fibers

spinning parameters	conditions
dope composition (NMP/ethanol/P84) (wt %)	64/10/26
dope flow rate (mL/min)	0.6
dope viscosity at 25 °C and shear rate 10/s (cP)	14402
bore fluid composition and coagulation bath	water
bore fluid flow rate (mL/min)	0.3
air gap (cm)	0, 1, 5, 10
spinning and coagulation bath temperature (°C)	25
takeup rate (cm/min)	free falling

For characterization purposes, fiber samples were immersed in liquid nitrogen, fractured, and then sputtered with platinum using a JEOL JFC-1300 platinum coater. A scanning electron microscope (SEM; JEOL JSM-5600LV) was employed to examine the cross section of all resulting fibers.

3. Results and Discussion

3.1. Types of Macrovoids. Figures 1−5 illustrate typical cross-section morphology of the as-spun hollow fiber membranes as a function of annulus gap and air gap distance. Figure 6 shows that there are at least four types of macrovoids: inward-pointed, outward-pointed, elliptical, and teardrop shapes. With enlarged pictures, one can clearly observe the residual traces of nonsolvent intrusion for some of the inward-pointed and outward-pointed macrovoids. The main causes of these types of macrovoids arise from surface instability, skin rupture, or convective flow during the rapid coagulation.[1,13−17] Once the nonsolvent intrudes, the depletion of the solvent from the spinning solution occurs rapidly. This is due to the fact that the solvent has a great tendency to diffuse to a lower chemical potential entity (i.e., nonsolvent coagulant). The semicoagulated or nascent skin would contract and reseal the intrusion points because of fluid elasticity and lowering surface energy, while the nucleation of depleted solvents in the polymer-lean phase takes place and forms the macrovoid.

The origins of elliptical and teardrop shape macrovoids are most likely from solutocapillary convection[22,23] or osmosis pressure[19] because of their similarity in shapes. However, based on Cabasso's observation,[16] the conical or teardrop macrovoids may also form from solution intrusion and subsequently membrane contraction. Since three or four types of macrovoid can coexist in Figure 6, this implies that several different mechanisms can take place simultaneously. Compared to the asymmetric flat membranes, more variables are involved in the macrovoid formation in the hollow fiber membranes.[16] One of the reasons is because, unlike flat sheet membrane casting, both outer and lumen sides of the hollow fiber membranes face the coagulation media (see Figure 9). Furthermore, the as-spun

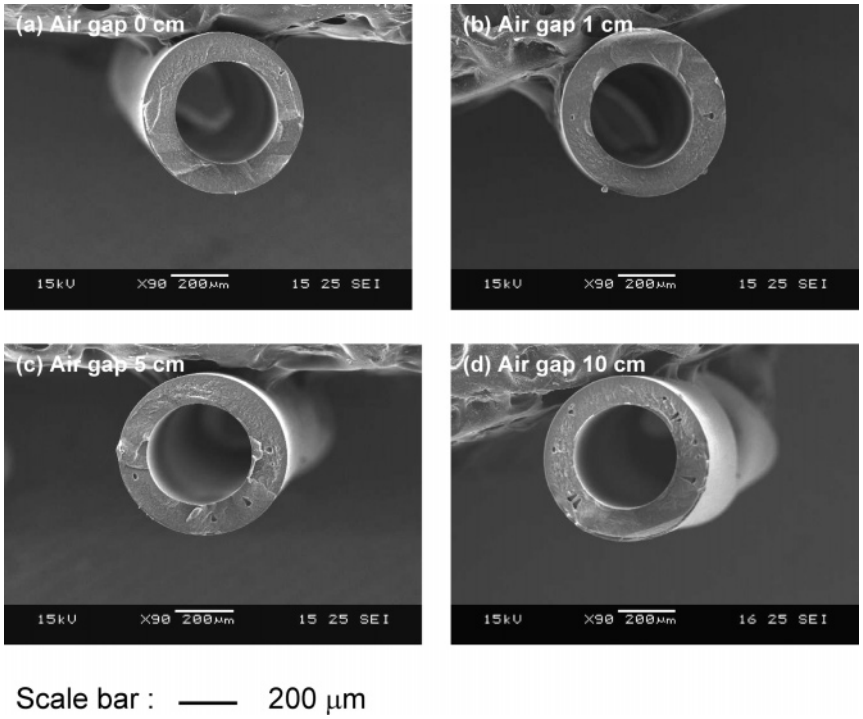

Figure 1. SEM images of cross sections of hollow fiber membranes spun at (a) 0, (b) 1, (c) 5, and (d) 10 cm air gaps using spinneret A. o.d. = 0.70 mm; i.d. = 0.50 mm; ΔD = 0.1 mm.

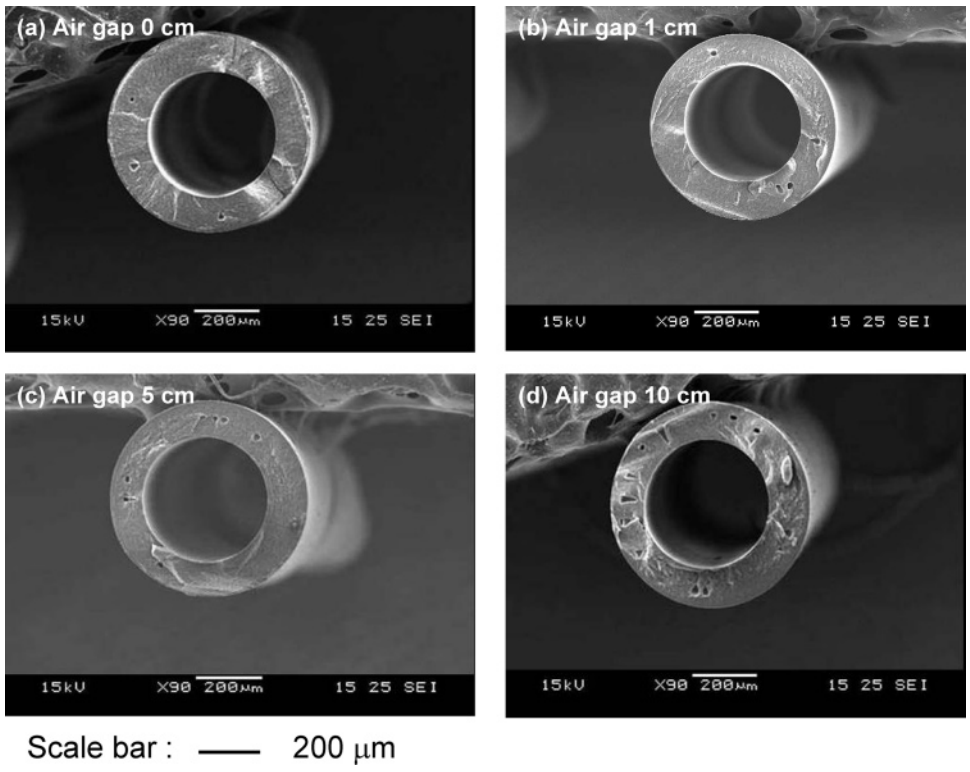

Figure 2. SEM images of cross sections of hollow fiber membranes spun at (a) 0, (b) 1, (c) 5, and (d) 10 cm air gaps using spinneret B. o.d. = 0.85 mm; i.d. = 0.50 mm; ΔD = 0.175 mm.

fibers also experience die swelling, relaxation, gravity, and spinning-line stress when exiting from the spinneret if there is an air gap before coagulation. Unless the experiments are well-designed, one cannot decouple shear, elongational, gravity, and coagulation effects on the hollow fiber formation.[49] Thus, the macrovoid formation in hollow fiber membranes appears much more complicated than in flat asymmetric membranes.

3.2. Macrovoids on the Cross-Sectional Morphology of Wet-Spun Hollow Fibers. Figure 7 displays macrovoids on the cross-section morphology of wet-spun hollow fibers. A thinner annulus gap results in a lesser number of macrovoids. Interestingly, the hollow fiber membranes spun from thinner annulus gaps (e.g., spinnerets A−C) show only inward-pointed macrovoids, while those spun using spinnerets D and E have both inward- and outward-pointed macrovoids. These observations on macrovoid formation vs spinneret annulus gap are somewhat in agreement with the previous works of Vogrin et al.[41] and Li et al.[42] on asymmetric flat membranes, where they

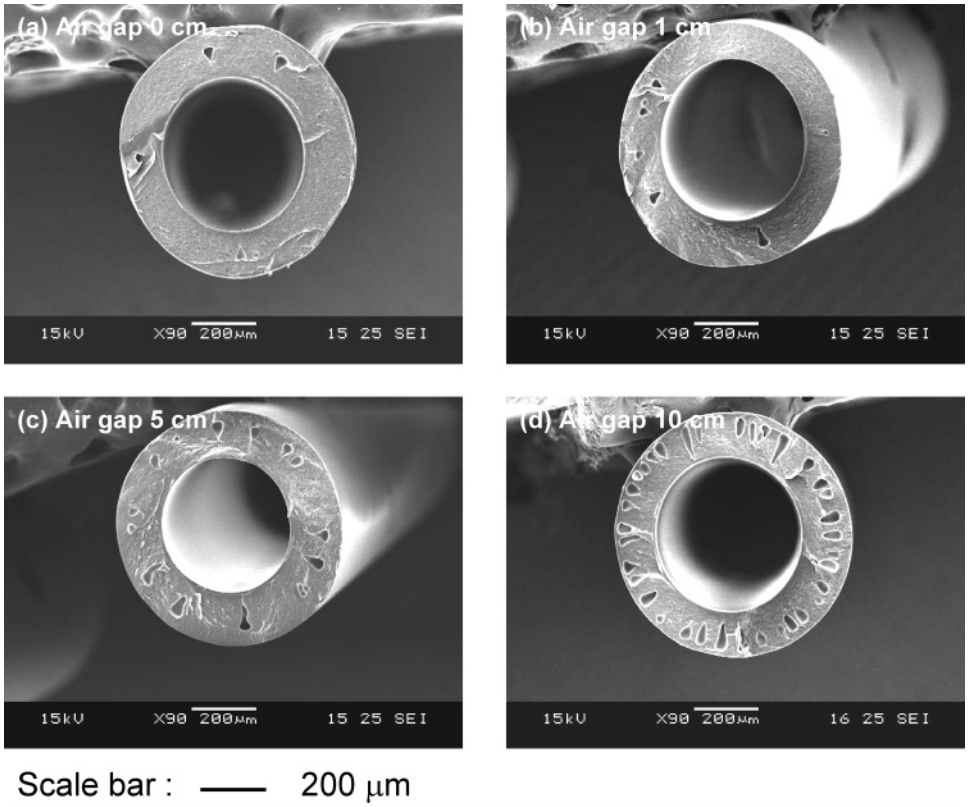

Figure 3. SEM images of cross sections of hollow fiber membranes spun at (a) 0, (b) 1, (c) 5, and (d) 10 cm air gaps using spinneret C. o.d. = 0.81 mm; i.d. = 0.30 mm; $\Delta D = 0.25$ mm.

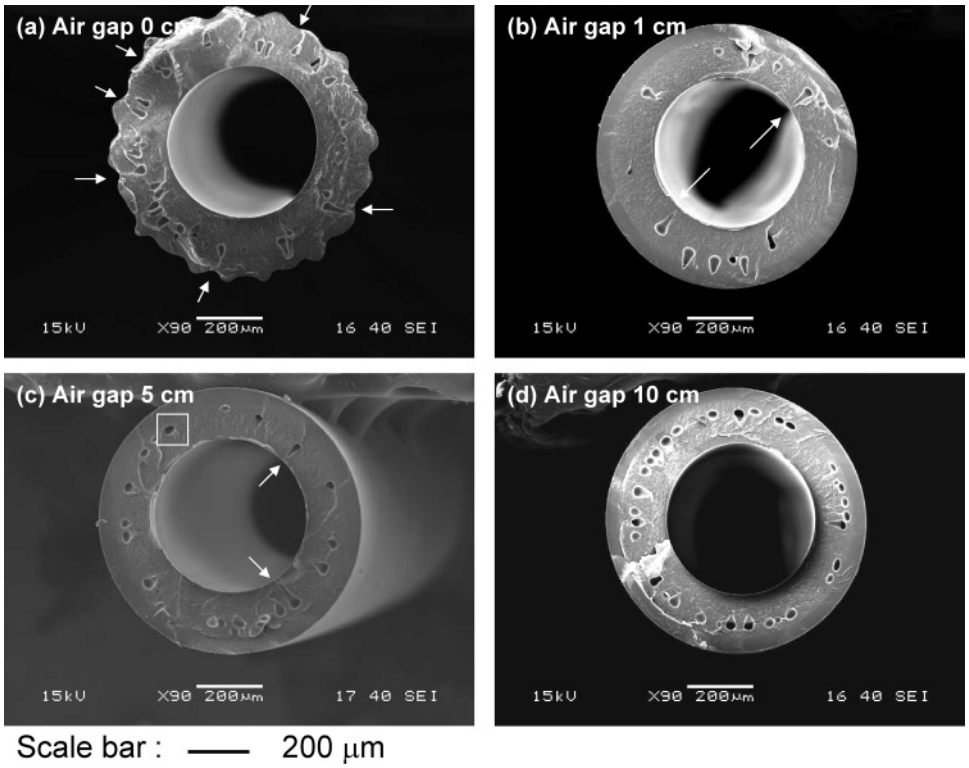

Figure 4. SEM images of cross sections of hollow fiber membranes spun at (a) 0, (b) 1, (c) 5, and (d) 10 cm air gaps using spinneret D. o.d. = 1.20 mm; i.d. = 0.50 mm; $\Delta D = 0.35$ mm. Arrows are traces of nonsolvent intrusion.

stated that there is a structure-transition thickness existing from a spongelike structure to macrovoid during the fabrication of flat membranes.

For P84 hollow fiber membranes spun from the 26/64/10 (wt %) P84/*N*-methylpyrrollidone (NMP)/ethanol mixture, the critical thickness is about 105 μm when the annulus gap of 0.05 mm is used. This value is much higher than our previous report on the asymmetric flat membranes[42] (i.e., 105 μm vs 11 $\pm$ 2 μm). This huge difference in the critical structure-transition thickness may possibly arise from two facts:

(1) The effects of different coagulation rates: The inner and outer skins of the wet-spun hollow fiber are coagulated almost

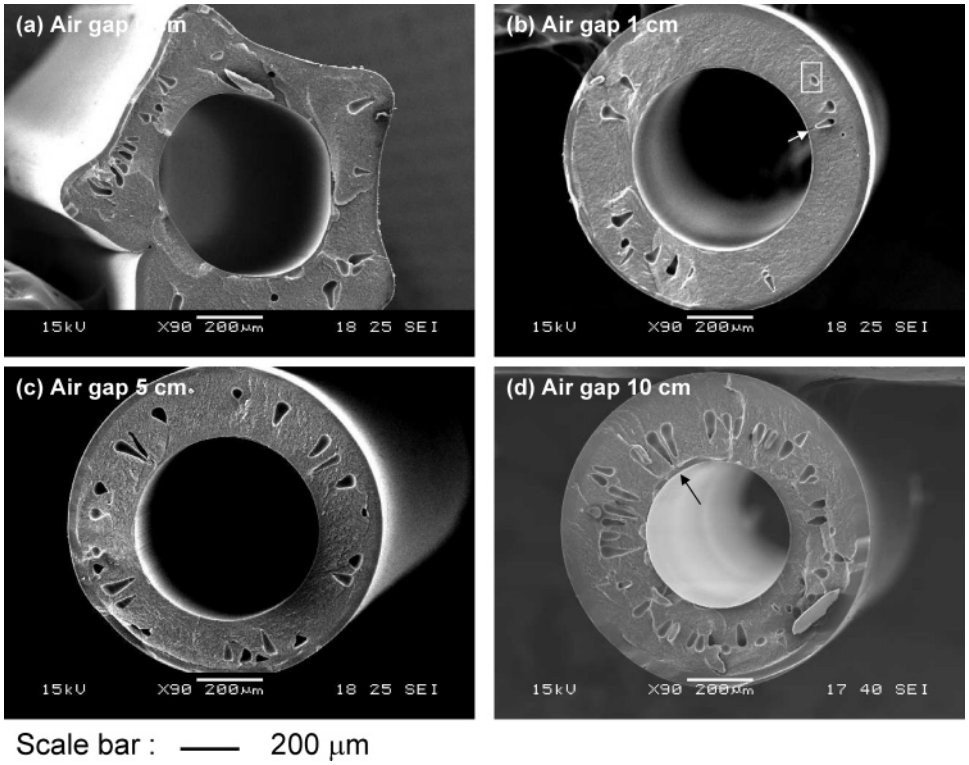

Figure 5. SEM images of cross sections of hollow fiber membranes spun at (a) 0, (b) 1, (c) 5, (d) 10 cm air gaps using spinneret E. o.d. = 1.50 mm; i.d. = 0.50 mm; $\Delta D = 0.50$ mm. Arrows are traces of nonsolvent intrusion.

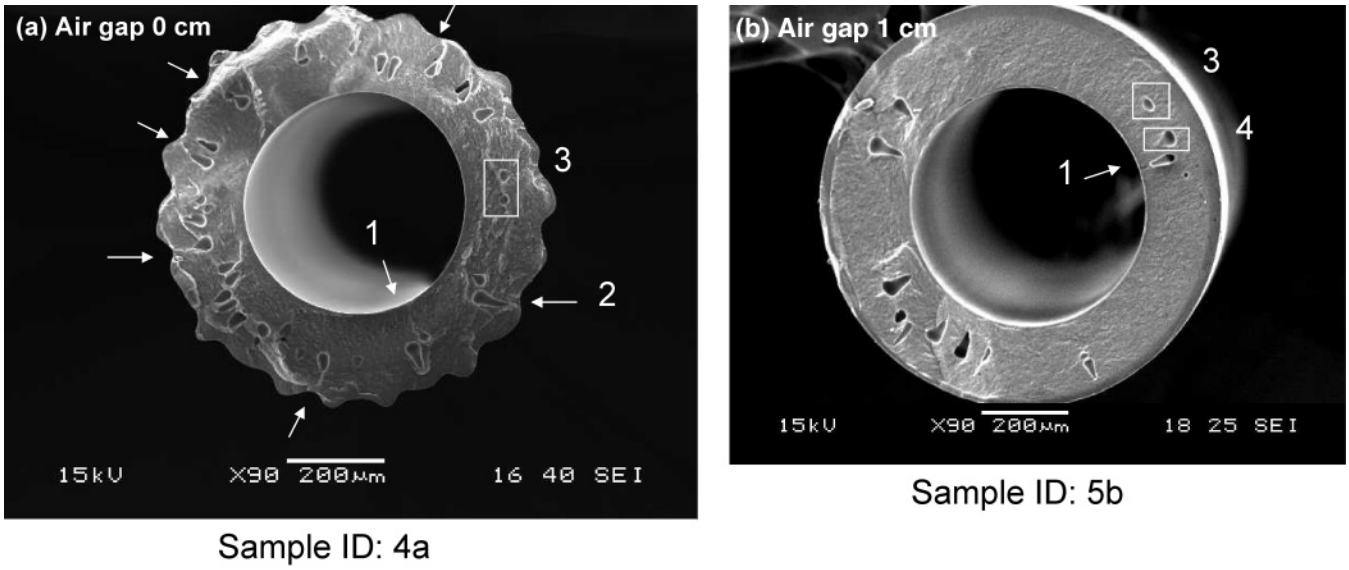

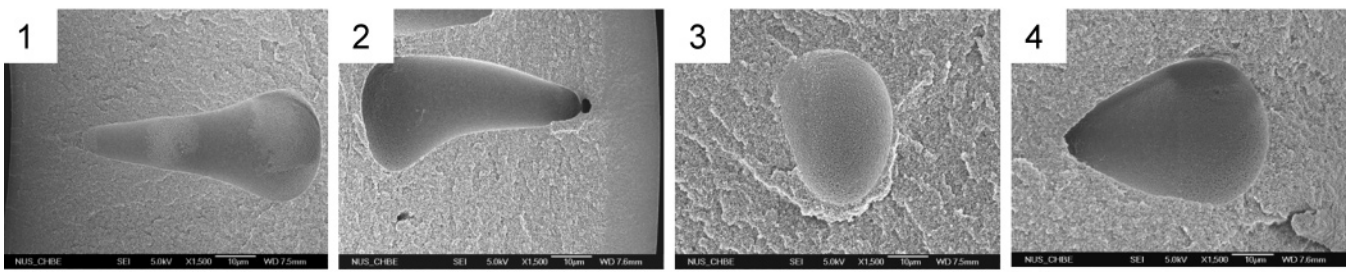

Figure 6. Four types of macrovoids and trace of intrusion: 1, inward-pointed; 2, outward-pointed; 3, elliptical; and 4, teardrop shape macrovoids.

immediately after exiting from the spinneret and precipitate in the coagulation bath filled with water, while the asymmetric flat membrane is cast on a glass plate with a free surface facing the air for a short period of time. As a result, the outer surface of the nascent flat membrane can move slightly up and down and accommodate the macrovoid formation via various mech-

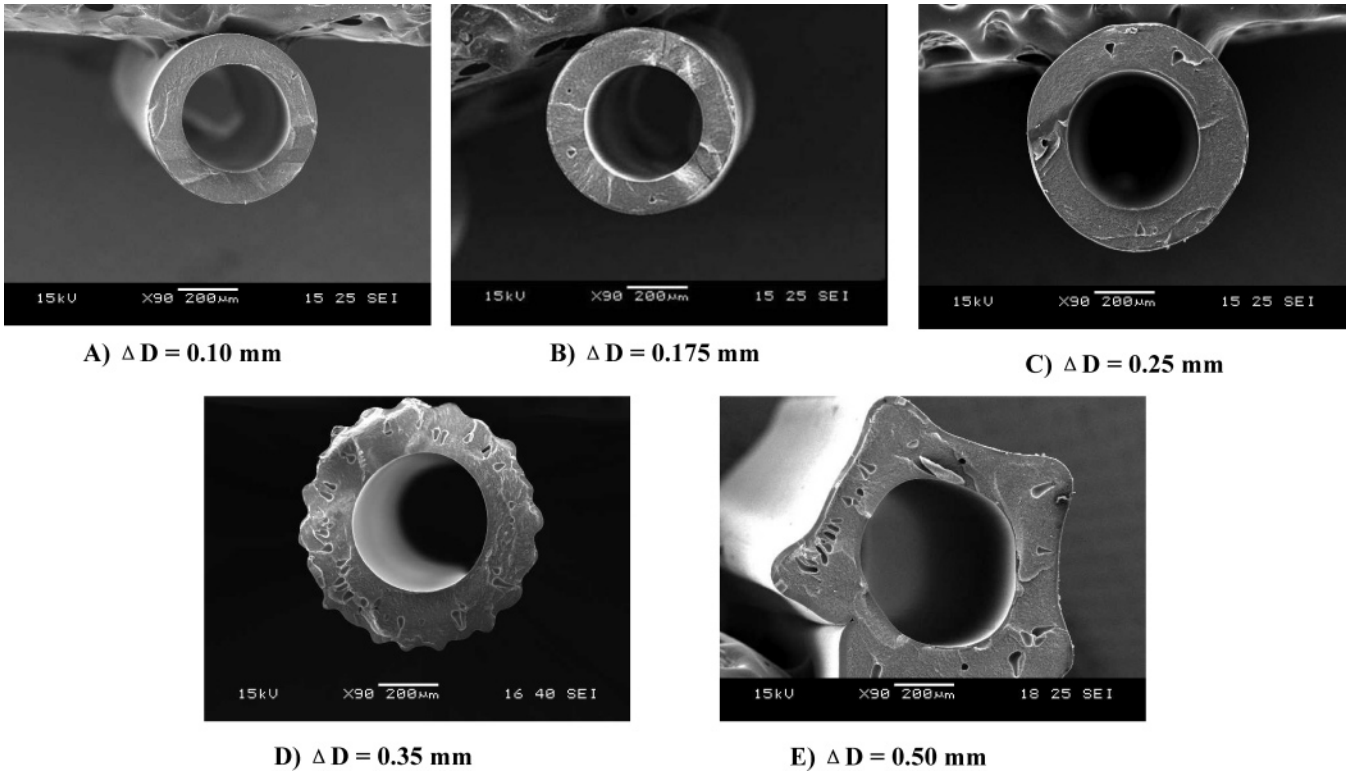

Figure 7. Cross sections of wet-spun hollow fibers (0 cm air gap).

anisms underneath the skin surface. The free surface and the easy accommodation for macrovoid formation in the asymmetric flat membrane may lower the critical structure-transition thickness. Section 3.3 will further discuss this issue.

(2) The effects of different shear stresses and chain packing: Compared with hollow fiber spinning, the asymmetric flat membrane experiences much less and shorter shear stress during the membrane casting. Previous studies have proved that shear stresses within the spinneret can effectively change the state of fluid[50] and suppress the macrovoid formation.[40,51] Therefore, hollow fibers extruding from a small annular gap would experience higher shear rates and stresses that would result in a higher molecular orientation and chain packing, both of which do not favor the macrovoid formation.

From a power-law fluid flowing through an annulus spinneret, the shear stress, τ_{rz}, may be expressed as follows:[47,48]

$$\tau_{rz} = -m\left|\frac{\mathrm{d}V_z}{\mathrm{d}r}\right|^{n-1}\frac{\mathrm{d}V_z}{\mathrm{d}r} \tag{2}$$

where r is the radial direction, z is the flow direction, m and n are parameters in the power-law viscosity model, and V_z is the velocity in the z direction. For the spinning dope solution, a relationship between shear stress τ (N m^{-2}) and shear rate γ (s^{-1}) is shown in eq 1. By combining the equation of velocity profile[47] and volumetric flow rate[47] of the power-law fluid in an annulus, the shear rate at the outer wall of the spinneret can be calculated as follows:[47,48,52]

$$\left|\frac{\mathrm{d}V_z}{\mathrm{d}r}\right|_{r=R} = \frac{Q}{\pi R^3}\frac{(1-\lambda^2)^s}{\int_k^1|\lambda^2-\rho^2|^{s+1}\rho^{-s}\,\mathrm{d}\rho} \tag{3}$$

where R is the radius of the annulus spinneret, k is the ratio of inner radius to outer radius of the spinneret, s is $1/n$, Q is the volume flow rate in an annulus, ρ is a dimensionless dummy variable, and λ is a dimensionless radial position where the velocity, V_z, is the maximum and its relationship with R obeys the equation of $r = \lambda R$.

Equations 2 and 3 indicate that an increase in annular gap (i.e., a lower k value and/or a large R value) results in a significant decrease in shear rate and stress at the outer skins, respectively. Although the residence time of a dope solution flowing through the annular channel is very short, the flow-induced shear rate and stress can significantly affect the rheological behavior of the polymeric solution, i.e., shift the spinodal curve,[53,54] because most highly concentrated polymeric solutions are viscoelastic fluids, i.e., non-Newtonian fluids. Regarding macrovoid formation, Wang et al.[51] suggested that the size of the long fingerlike macrovoids in their hollow fiber membranes spun with a 90° straight spinneret decreased with an increase of shear rate. When they further increased the dope flow rate to 3.0 mL/min or above, they found that most macrovoids disappeared. This is due to the fact that a higher shear rate and stress result in better molecular orientation and chain packing of the polymeric dope solution, which retards the penetration of external coagulant. Therefore, the macrovoid formation can be suppressed.

Basically, the decreased shear rate would lower the molecular orientation of the nascent fiber passing through the annular spinneret, while the decreased stress would reduce the molecular packing; both factors remove the barrier of macrovoid formation. Thus, wet-spun hollow fibers spun from thicker annulus gaps such as spinnerets D and E have both inward- and outward-pointed macrovoids mainly because of nonsolvent intrusion. The trace of intrusion can be visibly seen in the enlarged SEM pictures.

3.3. Effects of Air Gap Distance on Macrovoid Formation. 3.3.1. Inward-Pointed Macrovoids. Figure 8 depicts the effect of air gap distance on the number of inward-pointed long, elliptical, and teardrop shape macrovoids. Hollow fibers spun at shorter air gap distances, i.e., 0 or 1 cm, exhibit a lesser number of inward-pointed macrovoids compared to those spun

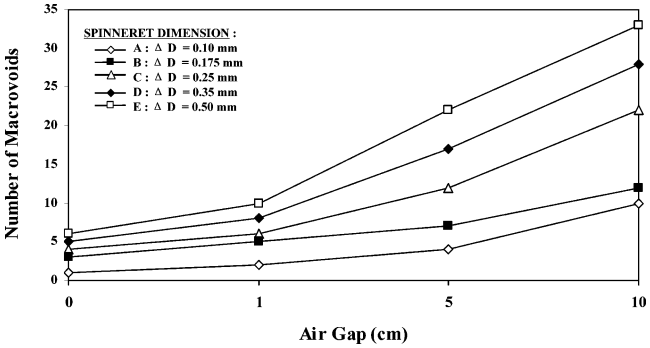

Figure 8. Effect of spinneret dimension and air gap distance on number of inward-pointed macrovoids.

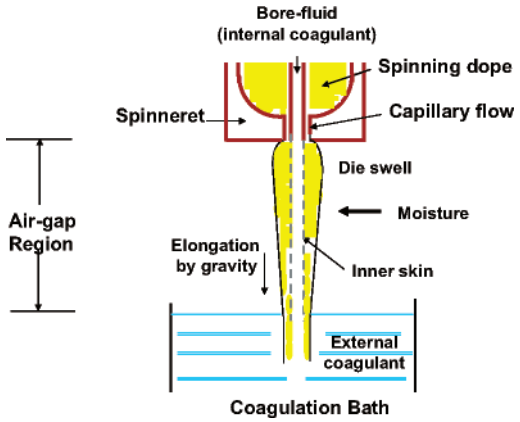

Figure 9. Coagulations in hollow fiber spinning.

at longer air gap distances, e.g., 5 or 10 cm. This relationship magnifies in the case of thicker annular spinneret gaps because a greater number of inward-pointed macrovoids can be observed for hollow fibers spun from thicker annulus gaps. In addition to nonsolvent intrusion, more elliptical and teardrop shape macrovoids appear in the cross sections of Figures 1d, 2d, 3d, 4d, and 5d. Their origins are most likely from solutocapillary convection.

As shown in Figure 9, it has been widely known that there are two coagulation paths in a dry-jet wet-spinning process. If water is chosen as the internal and external coagulants, the coagulation process in the lumen side may start immediately after extrusion of the dope solution from the spinneret, whereas slightly partial phase separation may occur in the external surface of the hollow fiber in the air gap region because of moisture-induced phase separation.[35,36] Only when the fiber is fully immersed in the coagulant bath may complete phase separation take place in the external surface of the fiber. Consequently, the inner side structure may be frozen almost instantaneously in the air gap region due to the usage of water as a strong internal coagulant. However, the outer layer skin structure has not been fixed yet. Therefore, similar to the case of fabricating flat asymmetric membranes, one may consider the extruded outer surface skin of hollow fiber membranes in the air gap region as a moving boundary surface, while the inner surface skin is considered as a fixed boundary surface.

Different solvent−nonsolvent exchanges take place at the outer and inner surfaces. NMP and water are highly miscible, but a rapid solvent exchange and polymer precipitation densify the inner skin that hinders a further movement of NMP to the lumen side. The early loss of NMP into the lumen side creates a steep concentration gradient across the membrane thickness, while the diffusion of water through the lumen side results in a localized homogeneous supersaturation solution. Both are

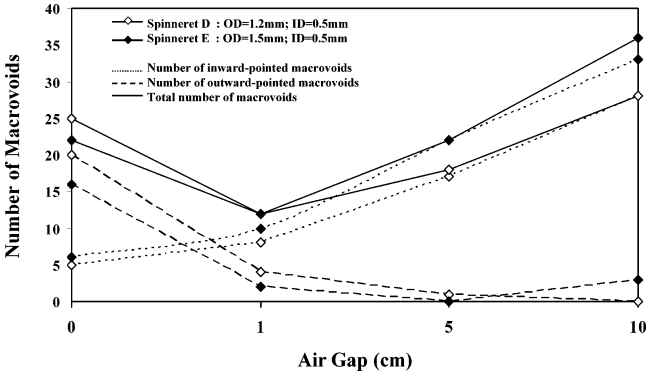

Figure 10. Effect of spinneret dimension and air gap distance on number of outward- and inward-pointed macrovoids using spinnerets D and E.

unstable and have a great tendency to be destabilized in order to lower their chemical potential. (For readers' information, a steep concentration and a localized homogeneous supersaturation solution are the prerequisites for the solutocapillary convection.[20−23]) On the other hand, the moisture-induced surface tension gradient and the die-swell-induced chain relaxation occur at the outer moving surface; both of them help drive the solutocapillary convection across the membrane thickness. Thus, an instantaneous liquid−liquid demixing occurs in the homogeneous supersaturation solution with the aid of solutocapillary convection and subsequently the nucleation of droplets in the polymer-lean phase forms the teardrop or elliptical shape macrovoids. Our previous works in solution spinning have indicated that the radial dimensional expansion of the outer fiber diameter during the die swell can be as high as 15%.[55] This large radial chain relaxation would definitely facilitate mass transfer and aid solutocapillary convection.

Since it takes time to induce solutocapillary convection through both the moisture-induced surface tension gradient and die swell-induced chain relaxation, hollow fibers spun at the lower air gap or without an air gap show only a few inward-pointed, elliptical, or teardrop shape macrovoids.

3.3.2. Outward-Pointed Macrovoids. As discussed in the previous section, the outward-pointed macrovoid gradually emerges when the outer layer channel thickness of a spinneret increases to 0.35 mm and above, i.e., in spinnerets D and E. Interestingly, the number of outward-pointed macrovoids becomes less with an increase in air gap distance as shown in Figure 10. This is due to the fact that the outward-pointed macrovoids in the wet-spun fibers or in those fibers spun from a short air gap distance are mainly caused by nonsolvent intrusion because of vigorous demixing, local surface instability, and skin rupture at the outer layer of the hollow fiber. As the air gap distance increases, the moisture-induced partial phase separation and the gravity-induced radial outflow due to an elongational drawing occur simultaneously. The former may create an ultrathin gel-like skin layer with a higher viscosity that is a barrier for nonsolvent intrusion,[35,36] while the latter induces a radial outer flow that hinders nonsolvent intrusion.[40] Consequently, as shown in the dashed lines of Figure 10, an increase in air gap distance diminishes the number of outward-pointed macrovoids.

During the dry-jet wet-spinning process, the gravity effect in the air gap region on membrane morphology is unavoidable. The axial elongation in the air gap will stretch the fiber in the flow or spinning direction. Thus, the nascent fiber will be stretched and becomes thinner. Therefore, from the perspective of the fiber, the bulk polymer moves inward. In other words, there is a radial inward movement of the polymer from the outer

surface (i.e., the free surface) to the inner side. This may squeeze out the spinning solvent within the fiber toward both the internal and external coagulants. As a consequence, it leads to a gravity-induced radial outflow phenomenon. The existence of gravity-induced and elongational-induced radial outflow and their effects on the membrane morphology have been verified recently.[40,55,56] It has been shown that hollow fibers spun at high elongational draw ratios can be free of macrovoids because the elongation-induced radial outflow prevents nonsolvent intrusion.[40] In addition, when spinning hollow fibers containing nanoparticles, it has been demonstrated the elongation-induced radial outflow can push nanoparticles toward the outer surface during the fabrication of dual-layer hollow fiber membranes[55] and alter the nanoparticle distribution across the membrane from a parabolic (∩) shape to a "U" (∪) shape in a single-layer hollow fiber membrane.[56]

Figure 10 also implies that the total number of macrovoids is not only dependent on the air gap distance, but also dependent on the annular gap of the spinneret. Clearly, many forces affecting macrovoid formation compete with one another starting from within the spinneret through the air gap region. One must take these factors into consideration for new hollow fiber membrane development.[36,40,51,55,56]

4. Conclusions

We have systematically investigated the effects of spinneret dimension and air gap distance on the macrovoid formation in the fabrication of P84 copolyimide hollow fiber membranes. The following conclusions can be made from this work:

(1) The critical structure-transition thickness from a sponge-like to a macroviod hollow fiber structure for this dope composition is about 105 μm, which is much larger than those reports for flat asymmetric membranes.

(2) Four types of macrovoids (inward- and outward-pointed, elliptical, and teardrop shapes) can be observed simultaneously in the hollow fiber membrane fabrication.

(3) Because of high shear rate and stress developed in a thin spinneret annulus gap, a thin annulus gap results in a lesser number of macrovoids than a thick one.

(4) When thin spinneret annulus gaps, i.e., from 0.05 to 0.25 mm, are used in the wet-spinning process, the inward-pointed macrovoids appear gradually with an increase in annulus gap, while both inward- and outward-pointed macrovoids are present in the fibers spun from larger spinneret dimensions, i.e., annulus gaps from 0.35 to 0.50 mm.

(5) The gravity-induced radial outflow, moisture-induced phase separation, and surface tension gradient have different effects on the formation of inward- and outward-pointed macrovoids. It is found that the number of inward-pointed macrovoids increases proportionally to the air gap distance while the number of outward-pointed macrovoids becomes less.

Acknowledgment

The authors are grateful to NUS for funding this research with Grant R-279-000-184-112. N.W. would like to thank UOP for the top-up support under Grant R-279-000-140-592. Thanks are also due to Prof. W. B. Krantz for his valuable input on the solutocapillary convection mechanism.

Literature Cited

(1) Craig, J. P.; Knudsen, J. P.; Holland, V. F. Characterization of Acrylic Fiber Structure. *Text. Res. J.* **1962**, *32*, 435.

(2) Loeb, S.; Sourirajan, S. Sea Water Demineralization by means of an Osmotic Membrane. *Adv. Chem. Ser.* **1963**, *38*, 117.

(3) Kesting, R. E.; Fritzsche, A. K. *Polymeric Gas Separation Membranes*; Wiley: New York, 1993.

(4) Cohen, C.; Tanny, G. B.; Prager, S. Diffusion-Controlled Formation of Porous Structures in Ternary Polymer Systems. *J. Polym. Sci., Polym. Phys.* **1979**, *17*, 477.

(5) Reuvers, A. J.; Van den Berg, J. W. A.; Smolders, C. A. Formation of Membranes by means of Immersion Precipitation. Part I: A Model to Describe Mass Transfer during Immersion Precipitation. *J. Membr. Sci.* **1987**, *34*, 45.

(6) Reuvers, A. J.; Smolders, C. A. Formation of Membranes by means of Immersion Precipitation. Part II: The Mechanism of Formation of Membranes Prepared from the System Cellulose Acetate−Acetone−Water. *J. Membr. Sci.* **1987**, *34*, 67.

(7) Smolders, C. A.; Reuvers, A. J.; Boom, R. M.; Wienk, I. M. Microstructures in phase-inversion membranes. Part 1. Formation of macrovoids. *J. Membr. Sci.* **1992**, *73*, 259.

(8) McHugh, A. J.; Yilmaz, L. The Diffusion Equation for Polymer Membrane Formation in Ternary Systems. *J. Polym. Sci., Polym. Phys.* **1985**, *23*, 1271.

(9) Yilmaz, L.; McHugh, A. J. Analysis of Nonsolvent-Solvent-Polymer Phase Diagrams and Their Relevance to Membrane Formation Modeling. *J. Appl. Polym. Sci.* **1986**, *31*, 997.

(10) Yao, C. W.; Burford, R. P.; Fane, A. G.; Fell, C. J. D. Effect of Coagulation Conditions on Structure and Properties of Membranes from Aliphatic Polyamides. *J. Membr. Sci.* **1988**, *38*, 113.

(11) Matz, R. The Structure of Cellulose Acetate Membranes 1. The Development of Porous Structures in Anisotropic Membranes. *Desalination* **1972**, *10*, 1.

(12) Frommer, M. A.; Messalam, R. M. Mechanism of membrane formation VI. Convective flows and large void formation during membrane precipitation. *Ind. Eng. Chem. Prod. Res. Dev.* **1973**, *12*, 328.

(13) Strathmann, H.; Kock, K.; Amar, P.; Baker, R. W. The formation mechanism of asymmetric membranes. *Desalination* **1975**, *16*, 179.

(14) Strathmann, H.; Kock, K. The formation mechanism of phase inversion membranes. *Desalination* **1977**, *21*, 241.

(15) Cabasso, I.; Klein, E.; Smith, J. K. Polysulfone Hollow Fibers. II. Morphology. *J. Appl. Polym. Sci.* **1977**, *21*, 165.

(16) Cabasso, I. Practice aspects in the development of a polymer matrix for ultrafiltration. In *Ultrafiltration Membranes and Applications*; Cooper, A. R., Ed.; Plenum Press: New York, 1980; p 57.

(17) Broens, L.; Altena, F. W.; Smolders, C. A.; Koenhen, D. M. Asymmetric membrane structures as a result of phase separation phenomena. *Desalination* **1980**, *32*, 33.

(18) Levich, V. G.; Krylov, V. S. Surface-Tension-Driven Phenomena. *Annu. Rev. Fluid Mech.* **1969**, *1*, 293.

(19) McKelvey, S. A.; Koros, W. J. Phase separation, vitrification, and the manifestation of macrovoids in polymeric asymmetric membranes. *J. Membr. Sci.* **1996**, *112*, 29.

(20) Ray, R. J.; Krantz, W. B.; Sam, R. L. Linear stability theory model for finger formation is asymmetric membranes. *J. Membr. Sci.* **1985**, *23*, 155.

(21) Paulsen, F. G.; Shojaieb, S. S.; Krantz, W. B. Effect of evaporation step on macrovoid formation in wet-cast polymeric membranes. *J. Membr. Sci.* **1994**, *91*, 265.

(22) Pekny, M. R.; Greenberg, A. R.; Khare, V.; Zartman, J.; Krantz, W. B.; Todd, P. Macrovoid pore formation in dry-cast cellulose acetate membranes: buoyancy studies. *J. Membr. Sci.* **2002**, *205*, 11.

(23) Pekny, M. R.; Zartman, J.; Krantz, W. B.; Greenberg, A. R.; Todd, P. Flow-visualization during macrovoid pore formation in dry-cast cellulose acetate membranes. *J. Membr. Sci.* **2003**, *211*, 71.

(24) Lai, J. Y.; Lin, F. C.; Wu, T. T.; Wang, D. M. On the formation of macrovoids in PMMA membranes. *J. Membr. Sci.* **1999**, *155*, 31.

(25) Wang, D. M.; Lin, F. C.; Wu, T. T.; Lai, J. Y. Formation mechanism of the macrovoids induced by surfactant additives. *J. Membr. Sci.* **1998**, *142*, 191.

(26) Won, J.; Park, H. C.; Kim, U. Y.; Kang, Y. S.; Yoo, S. H.; Jho, J. Y. The effect of dope solution characteristics on the membrane morphology and gas transport properties: PES/g-BL/NMP system. *J. Membr. Sci.* **1999**, *162*, 247.

(27) Fritzsche, A. K.; Arevalo, A. R.; Moore, M. D.; O'Harab, C. The surface structure and morphology of polyacrylonitrile membranes by atomic force microscopy. *J. Membr. Sci.* **1993**, *81*, 109.

(28) Chung, T. S.; Kafchinski, E. R. The effects of spinning conditions on asymmetric 6FDA/6FDAM polyimide hollow fibers for air-separation. *J. Appl. Polym. Sci.* **1997**, *65*, 1555.

(29) Chung, T. S.; Hu, X. D. Effect of air-gap distance on the morphology and thermal properties of polyethersulfone hollow fibers. *J. Appl. Polym. Sci.* **1997**, *66*, 1067.

(30) Jiang, L. Y.; Chung, T. S.; Li, D. F.; Cao, C.; Kulprathipanja, S. Fabrication of Matrimid/polyethersulfone dual-layer hollow fiber membranes for gas separation. *J. Membr. Sci.* **2004**, *240*, 91.

(31) Liu, Y.; Koops, G. H.; Strathmann, H. Characterization of morphology controlled polyethersulfone hollow fiber membranes by the addition of poly(ethylene glycol) to the dope and bore fluid solution. *J. Membr. Sci.* **2003**, *223*, 187.

(32) Li, D. F.; Chung, T. S.; Wang, R. Morphological aspects and structure control of dual-layer asymmetric hollow fiber membranes formed by a simultaneous co-extrusion approach. *J. Membr. Sci.* **2004**, *243*, 53.

(33) Lin, K. Y.; Wang, D. M.; Lai, J. Y. Nonsolvent-Induced Gelation and Its Effect on Membrane Morphology. *Macromolecules* **2002**, *35*, 6697.

(34) Won, J.; Lee, H. J.; Kang, Y. S. The effect of dope solution characteristics on the membrane morphology and gas transport properties: 2. PES/g-BL system. *J. Membr. Sci.* **2000**, *176*, 11.

(35) Chung, T. S.; Hu, X. Effect of air-gap distance on the morphology and thermal properties of polyethersulfone hollow fibers. *J. Appl. Polym. Sci.* **1997**, *66*, 1067.

(36) Tsai, H. A.; Kuo, C. Y.; Lin, J. H.; Wang, D. M.; Deratani, A.; Pochat-Bohatier, C.; Lee, K. R.; Lai, J. Y. Morphology control of polysulfone hollow fiber membranes via water vapor induced phase separation. *J. Membr. Sci.* **2006**, *278*, 390.

(37) Tsai, H. A.; Li, L. D.; Lee, K. R.; Wang, Y. C.; Li, C. L. Effect of surfactant addition on the morphology and pervaporation performance of asymmetric polysulfone membranes. *J. Membr. Sci.* **2000**, *176*, 97.

(38) Chung, T. S.; Kafchinski, E. R. The effects of spinning conditions on asymmetric 6FDA/6FDAM polyimide hollow fibers for air-separation. *J. Appl. Polym. Sci.* **1997**, *65*, 1555.

(39) Ren, J. Z.; Chung, T. S.; Li, D. F.; Wang, R.; Liu, Y. Development of asymmetric 6FDA-2,6 DAT hollow fiber membranes for CO_2/CH_4 separation-1. The influence of dope composition and rheology on membrane morphology and separation performance. *J. Membr. Sci.* **2002**, *207*, 227.

(40) Wang, K. Y.; Li, D. F.; Chung, T. S.; Chen, S. B. The observation of elongation dependent macrovoid evolution in single and dual-layer asymmetric hollow fiber membranes. *Chem. Eng. Sci.* **2004**, *59*, 4657.

(41) Vogrin, N.; Strpnik, C.; Musil, V.; Brumen, M. The wet phase separation: the effect of cast solution thickness on the appearance of macrovoids in the membrane forming ternary cellulose acetate/acetone/water system. *J. Membr. Sci.* **2002**, *207*, 139.

(42) Li, D. F.; Chung, T. S.; Ren, J.; Wang, R. Thickness dependence of macrovoid evolution in wet phase-inversion asymmetric membranes. *Ind. Eng. Chem. Res.* **2004**, *43*, 1553.

(43) Baker, R. W. Future Directions of Membrane Gas Separation Technology. *Ind. Eng. Chem. Res.* **2002**, *41*, 1393.

(44) Pearson, J. R. A. *Mechanics of Polymer Processing*; Elsevier Applied Science Publishers: London, 1985; p 190.

(45) Crochet, M. J., Davies, A. R.; Walters, K. *Numerical Simulation of Non-Newtonian Flow*; Elsevier: New York, 1984; p 236.

(46) Qiao, X. Y.; Chung, T. S.; Pramoda, K. P. Fabrication and characterization of BTDA-TDI/MDI (P84) co-polyimide membranes for the pervaporation dehydration of isopropanol. *J. Membr. Sci.* **2005**, *264*, 176.

(47) Bird, R. B.; Steward, W. E.; Lighfoot, E. N. *Transport Phenomena*, 1st ed.; Wiley: New York, 1960.

(48) Bird, R. B.; Amstrong, R. C.; Hassager, O. *Dynamics of Polymeric Liquids, Vol. 1. Fluid Mechanics*, 2nd ed.; Wiley: New York, 1987.

(49) Chung, T. S.; Teoh, S. K.; Lau, W. W. Y.; Srinivasan, M. P. Effect of shear stress within the spinneret on hollow fiber membrane morphology and separation performance. *Ind. Eng. Chem. Res.* **1998**, *37*, 3930; *Ind. Eng. Chem. Res.* **1998**, *37*, 4903.

(50) Wolf, B. A. Thermodynamic theory of flowing polymer solutions and its applications to phase separation. *Macromolecules* **1984**, *17*, 615.

(51) Wang, K. Y.; Matsuura, T.; Chung, T. S.; Guo, W. F. The effects of flow angle and shear rate within the spinneret on the separation performance of poly(ethersulfone) (PES) ultrafiltration hollow fiber membranes. *J. Membr. Sci.* **2004**, *240*, 67.

(52) Qin, J. J.; Wang, R.; Chung, T. S. Investigation of shear stress effect within a spinneret on flux, separation and thermomechanical properties of hollow fiber ultrafiltration membranes. *J. Membr. Sci.* **2000**, *175*, 197.

(53) Criado-Sancho, M.; Casas-Vazquez, J.; Jou, D. Hydrodynamic interaction and the shear induced shift of the critical point in polymer solutions. *Polymer* **1995**, *21*, 4107.

(54) Criado-Sancho, M.; Jou, D.; Casas-Vazquez, J. Definition of non-equilibrium chemical potential: phase separation of polymers in shear flow. *Macromolecules* **1991**, *24*, 2834.

(55) Jiang, L. Y.; Chung, T. S.; Cao, C.; Huang, Z.; Kulprathipanja, S. Fundamental understanding of nano-sized zeolite distribution in the formation of the mixed matrix single- and dual-layer asymmetric hollow fiber membranes. *J. Membr. Sci.* **2005**, *252*, 89.

(56) Xiao, Y. C.; Wang, K. Y.; Chung, T.-S.; Tan, J. Evolution of Nano-Particle Distribution during the Fabrication of Mixed Matrix TiO_2-Polyimide Hollow Fiber Membranes. *Chem. Eng. Sci.* **2006**, *61*, 6228−6233.

Received for review May 25, 2006
Revised manuscript received July 19, 2006
Accepted August 8, 2006

IE0606587